Materials Science in Semiconductor Processing 74 (2018) 342–346

Contents lists available at ScienceDirect

Materials Science in Semiconductor Processing

journal homepage: www.elsevier.com/locate/mssp

The electrical properties and distribution of indium in germanium crystals

Guojian Wang[a,*], Hao Mei[a], Xianghua Meng[a,b], Dongming Mei[a], Gang Yang[a]

[a] Department of Physics, University of South Dakota, Vermillion, SD 57069, USA
[b] Department of Chemistry, University of South Dakota, Vermillion, SD 57069, USA

ARTICLE INFO

Keywords:
Segregation
Czochralski method
Semiconducting germanium

ABSTRACT

Indium doped germanium crystals were grown in a hydrogen atmosphere using the Czochralski method. The electrical properties of indium doped germanium crystals were measured by Hall effect at 77 K. The axial and radial distributions of indium in the germanium crystals were investigated. The effective segregation coefficient of indium in germanium is determined to be 0.0009 with the concentration of indium from 3×10^{12}~1×10^{19} cm^{-3}. The interface shape between melt and crystal determined the radial distribution of indium in germanium crystals.

1. Introduction

Germanium crystals have a wide field of applications such as windows and lenses for IR optics, radiation detectors and substrates for high efficiency solar cells. The impurities will have effect on the electrical and optical properties of germanium. The group III elements (Boron, Aluminum, Gallium and Indium) are acceptor (p type) impurities in germanium crystal. Recently, the diffusion and implantation of indium in germanium have attracted intensive research interests [1–4]. As a p type dopant, the electrical properties and distribution of indium in germanium crystals had been studied in 1950s and 1960s [5,6]. At that time, the impurities in germanium raw ingot were higher than 10^{13} cm^{-3}. Even now, it is very difficult task to purify germanium ingot to impurity level lower than $< 10^{12}$ cm^{-3} that only few commercial companies (Umicore, Ortec, and Canberra) and a research group at the University of South Dakota [7–9] have achieved. Therefore, the electrical properties and distribution of indium in germanium crystal were investigated with doping level higher than 10^{13} cm^{-3} [10,11]. The original impurities in germanium ingot could bring in errors in the study of properties of target dopant in germanium crystal and make the analysis complicated when the doping level $< 10^{13}$ cm^{-3}.

Normally, the germanium crystals were grown in an inert atmosphere (like Helium and Argon) in graphite crucible by Czochralski method [12,13]. Graphite crucible contains boron and aluminum [14], which can be dissolved into germanium melt to increase the impurity concentration. High purity quartz crucibles have been verified to be the best container for germanium melt. Therefore, it is used for growing high purity germanium crystals [15]. However, the germanium can react with quartz crucible to bring the oxygen into germanium melt. Oxygen can form oxidation complexes acting as trap centers to affect the energy resolution of the germanium gamma ray detectors. Experiments showed when the doping level of boron and aluminum is lower than 10^{12} cm^{-3}, the effective segregation coefficient for boron disappears faster than the prediction by a theoretical model [14] and for aluminum approaches one, which is caused by boron and aluminum oxidation complexes [16–18]. When germanium crystal is grown in a hydrogen atmosphere, the concentration of oxygen in germanium crystal can be reduced. It will be interesting to study if the distribution of indium would be affected by the possible oxidation complexes.

Diameter of 3–12 cm high purity germanium crystals (impurity level $< 10^{11}$ cm^{-3}) have been grown in our group [7,8,19,20]. We can use highly pure germanium ingots to study the distribution and electrical properties of indium in germanium crystals. According to our knowledge, the distribution of indium in germanium crystal with doping level around 10^{12} cm^{-3} has not been investigated. Therefore, in this paper, we report the indium doped germanium crystal growth, the impact of indium concentration on the Hall mobility at 77 k, and the axial and radial distribution of indium in the germanium crystals.

2. Experiment

High-purity Germanium ingots (p-type with net carrier concentration $< 2 \times 10^{11}$ cm^{-3} at 77 K) of 3 kg in mass were charged in to a quartz crucible, which is 18 cm in diameter and 11 cm in depth. Indium (with a purity of 99.9999%) rods with doping concentration 2.94×10^{15} cm^{-3} and 9.73×10^{18} cm^{-3} were added to the crucible for each Ge crystal. Two < 100 > oriented germanium crystals with 8–9 cm in

* Corresponding author.
E-mail address: guojian.wang@usd.edu (G. Wang).

https://doi.org/10.1016/j.mssp.2017.11.004
Received 18 August 2017; Received in revised form 26 October 2017; Accepted 2 November 2017

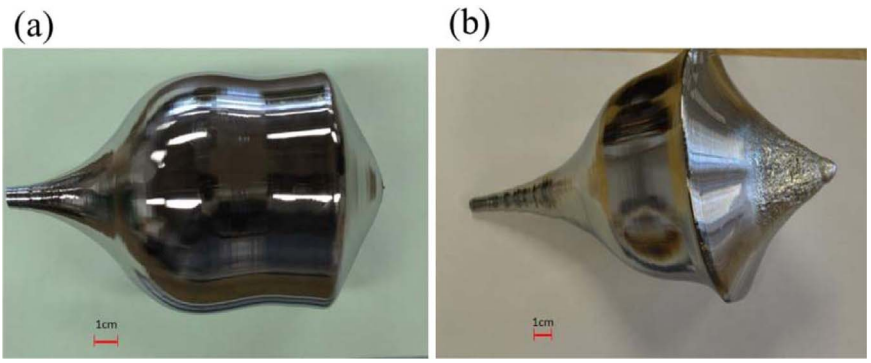

Fig. 1. (a) Crystal A with indium doping concentration 2.94 × 10^{15} cm^{-3} (b) Crystal B with indium doping concentration 9.73 × 10^{18} cm^{-3}.

diameter were grown by CZ (Czochralski) method at a pulling rate of 25 mm/h in a flowing gas atmosphere of high purity H_2 (5 N) with a flux of 150 l/h under a pressure of 1 atm. The rotation speed of the crystals was 3 rpm. In the finishing process, all the germanium melt must be pulled out completely; otherwise, the remaining melt will break the quartz crucible.

Fig. 1 shows the grown crystals. These crystals were cut into wafers at various positions along the grown axis by a diamond wire saw. Then, square specimens (1.5 × 1.5 × 0.15 cm^3) were cut from the wafers along the radial direction. These samples were polished, ultrasonically washed in a methanol, etched in HNO_3: HF (1:3) solution for 3 min, rinsed with deionized water, and dried with nitrogen gas. Ga-In (75.5:24.5 wt%) eutectic ohmic contacts were then scratched onto the four corners of the samples to be electrodes for Hall effect measurement. Finally, the samples were measured at 77 K (liquid N_2 temperature) using the Hall effect with the Van der Pauw geometry. An Ecopia HMS-3000 with a 0.55 T permanent magnet was used to make the measurements.

3. Hall effect of indium doped germanium crystals

According to the empirical expression for the intrinsic charge carrier density by Conwell [21], the numbers of free charge carriers are 2.5 × 10^{13} cm^{-3} at room temperature (300 K) and 1.9 × 10^{-6} cm^{-3} at liquid nitrogen temperature (77 K) for germanium. At 77 K, the group III and V elements are completely ionized impurities in germanium [22]. Hall effect measurement is an effective method to measure ionized impurities in germanium. Therefore, the Hall effect measurement can be used for measuring the indium concentration in germanium at 77 K without the interference from thermal generated free charge carriers.

The active-impurity concentration (N_A-N_D) is given by:

$$N_A - N_D = r/(\rho e \mu_{H(norp)}), \tag{1}$$

and

$$N_A - N_D = r/(eR_H), \tag{2}$$

where N_A is the concentration of acceptor (hole); N_D is the concentration of donor (electron); ρ is the resistivity; e is the electron charge, 1.6 × 10^{-19} C; μ_H is the Hall mobility associated with the carrier type of sample, n or p, according to whether R_H is negative or positive, respectively; r is Hall effect factor and depends on temperature, crystal type and crystal orientation; and R_H is the Hall coefficient.

The n type impurity is mainly phosphorus with concentration < 10^{11} cm^{-3} [7] and the p type impurities like gallium and aluminum are less than 2 × 10^{11} cm^{-3}. The total amount of other impurities is much less than the concentration of indium in grown crystals. The charge carriers are made predominantly of holes from the ionized indium atoms. Therefore, Eqs. (1) and (2) are modified to be:

$$N_A = r/(\rho e \mu_p), \tag{3}$$

and

$$N_A = r/(eR_H) \tag{4}$$

Hall coefficient R_H is measured in terms of the voltage produced across the Hall probes, per unit magnetic field (B) and current (I):

$$R_H = \frac{\Delta V t}{IB} \tag{5}$$

where ΔV is the Hall voltage, t the thickness of the plate along the magnetic field.

According to Eqs. (3) and (4), the Hall mobility is determined by:

$$R_H = \rho \mu_H \tag{6}$$

The Hall mobility μ_H is related to the drift mobility μ by:

$$\mu_H = r\mu \tag{7}$$

where r is the Hall effect factor, which is 1.15 at 77 K for hole [23]. The poor contacts, effects of surface charge, macroscopic nonuniformity and inhomogeneities can make the measured Hall mobility lower than true values.

At 77 K, the drift mobility (μ) of hole in germanium is dominated by lattice-scattering mobility (μ_L) and ionized impurity scattering mobility (μ_I) [10,24]. The contribution of ionized impurity scattering mobility to the measured mobility can be estimated from Matthiessen's rule if the lattice-scattering mobility can be determined:

$$\frac{1}{\mu} = \frac{1}{\mu_L} + \frac{1}{\mu_I} \tag{8}$$

For holes, the lattice scattering mobility $\mu_L = 1.05 \times 10^9\, T^{-2.33}$ [23], at 77 K, μ_L = 42234 cm^2/vs which is close to the IEEE standard [25]. The ionized impurity scattering mobility can be calculated by Brooks-Herring equation [26,27]:

$$\mu_I = \frac{128\sqrt{2}\pi^{1/2}(\varepsilon_0\varepsilon_r)^2(k_B T)^{3/2}}{m^{*1/2}N_I Z^2 e^3}\left(\ln\frac{24m^*\varepsilon_0\varepsilon_r(k_B T)^2}{N_I e^2\hbar^2}\right)^{-1} \tag{9}$$

where N_I is the ionized impurity concentration, ε_0 is free space permittivity, ε_r is the relative permittivity of Ge, $m^* = 0.2\, m_0$ is the effective mass of hole [28], m_0 is the electron mass, $Z = 1$ is the effective charge number in Ge, k_B is the Boltzmann constant, and T is the temperature in Kevin.

The theoretical Hall mobility can be calculated by Eqs. (7)–(9) and is shown in Fig. 2. The measured Hall mobility has a good consistence with the calculated results. Thus the measured carrier concentrations of indium by Van der Pauw method are reliable.

4. The radial and axial distribution of indium doped in germanium crystals

Fig. 3 shows the radial distribution of indium concentration in different location of wafers. Center samples show lower indium concentration in comparing to the edge of samples. The indium concentration ratios of center and edge samples at different axial location (g) are shown in Table 1. The non-uniform radial distribution is caused

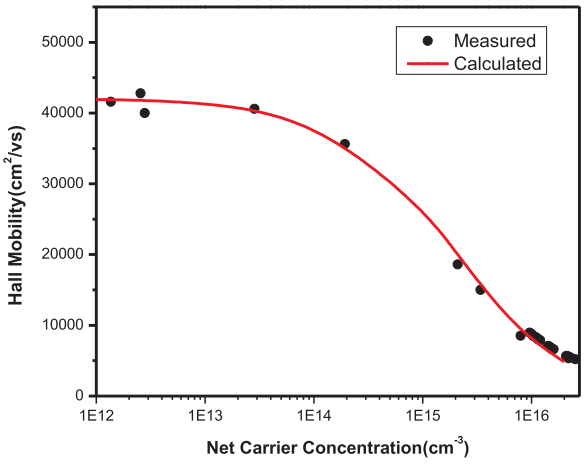

Fig. 2. The comparison of calculated and measured Hall mobility.

by the interface shape between crystal and melt, and the small segregation coefficient (< 1) of indium in germanium crystals.

In order to understand the interface shape between crystal and melt, a vertical section sample was cut, etched and taken a picture paralleling to the growth direction < 100 > by Olympus BX40 microscope, as shown in Fig. 4. This picture indicates the interface between crystal and melt is convex to the melt and, at this interface, the impurities are expected to be uniformly distributed. Therefore, the center of a sample wafer cut from a crystal would have solidified before the edge. This is the reason why the indium concentration level of center is higher than that of edge on the same wafer. The convex interface will generate stress in grown crystals. Raman spectroscopy can be used to measure the residual stress in Ge crystals [29,30]. Fig. 5 shows the measured Raman spectra from neck, center samples of wafer g = 0.097 and g = 0.60 for crystal A. The unstressed Raman peak is around 300.7 cm^{-1} [29,31]. The residual stress τ can be calculated by the equation [29]:

$$\tau = (0.4kbar{\cdot}cm) \times \Delta\omega(cm^{-1}) \quad (10)$$

where Δω is the shift of Gaussian fitted Raman peak away from the unstressed Raman peak. The calculated residual stress is listed in Table 2. The stress will bring in dislocations in grown crystals. Three samples from neck and centers of g = 0.097, and g = 0.60 wafers of the crystal A were etched by an etchant (48 wt% HF: 69.5 wt% HNO_3: acetic acid = 1:10:11 with 30 mg I_2 dissolved) to count the dislocation densities, which are shown in Fig. 6. The dislocation density is around 3300–7500 cm^2 in crystal A. The crystal B showed similar amounts of dislocation density and is not be shown here. Fritzsche et. al. found the

Table 1
The indium concentration ratios of center and edge samples, and interface heights at different axial location g for crystal A and B.

Crystal A			Crystal B		
Axial location g	N_{edge}/N_{center}	Interface height h (cm)	Axial location g	N_{edge}/N_{center}	Interface height h (cm)
0.097	1.14	1.09	0.072	1.06	0.52
0.22	1.08	0.52	0.223	1.09	0.63
0.40	1.10	0.52	0.435	1.12	0.57
0.60	1.10	0.30	0.629	1.08	0.18
0.91	1.23	0.05	0.849	1.12	0.41

dislocation densities up to 10^4 cm^{-2} will not affect impurity conduction in p type germanium [32]. Therefore, the residual stress will not have effect on Hall effect measurement.

The width of center sample is 1.5 cm, which is much smaller than the crystal diameter 8–9 cm. The mass ratio for the entire wafer is very close to the solidification fraction (*g*) at the center of the wafer. Therefore, the indium concentrations in the center samples at different location in the crystals are used for the calculation of segregation coefficient for indium. The data shown in Fig. 7 can be fitted by the Pfann's equation as follow [33]:

$$N(g) = kN_0(1-g)^k - 1 \quad (11)$$

where *N(g)* is the concentration of indium in the grown Ge crystal with a solidification fraction *g* and an effective segregation coefficient *k*. N_0 is an initial indium concentration in the melt. The variation of indium concentration in the grown crystals is well fitted using effective segregation coefficient $k = 0.0009 \pm 0.00001$ for the two crystals with different concentration of growth initiation N_0 2.94×10^{15} cm^{-3} and 9.73×10^{18} cm^{-3}, respectively. The effective segregation coefficient is close to other experimental value 0.001 [5,6] and theoretical value 0.0008 [34]. The normal segregation of indium indicates there is no significant reaction between the crucible material (SiO_2) and indium under hydrogen atmosphere. If indium can react with SiO_2, the products will be In_2O_3 or In_2O for indium, and SiO or Si for SiO_2. Four possible reactions are listed in Table 3. The Gibbs free energy can be used to judge the possibility of these reactions. The Gibbs free energy at 1210 K (melting point of Ge) can be expressed in the following equation:

$$\Delta G_{(1210K)} = \Delta G^{\circ}_{(1210K)} - RTLnK_{eq} \quad (12)$$

where $\Delta G^{\circ}_{(1210K)}$ is standard Gibbs free energy, $\Delta G_{(1210K)}$ is Gibbs free energy, *R* is gas constant (8.314 $J{*}K^{-1}$ mol^{-1}), *T* is temperature, and

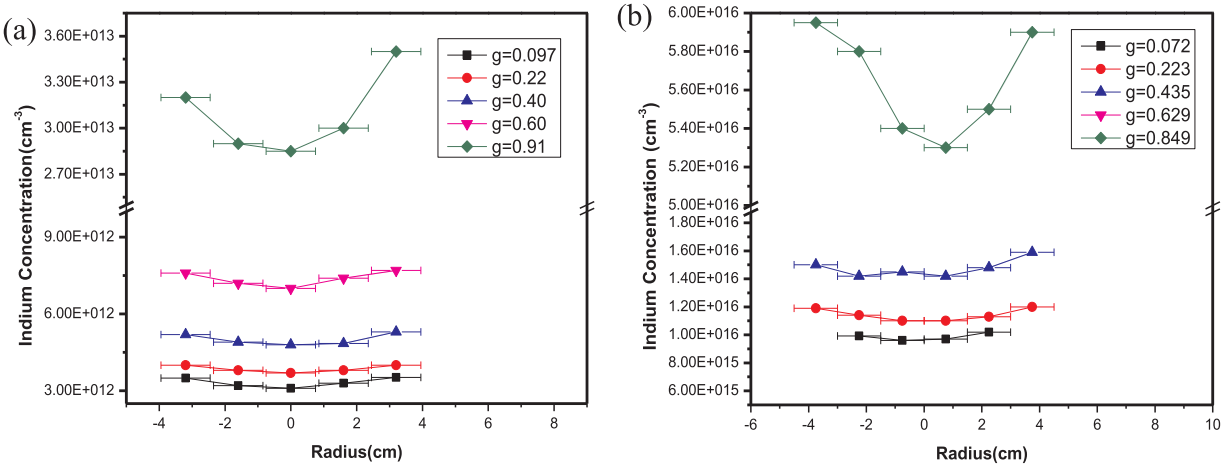

Fig. 3. (a) The radial distribution of indium in germanium crystal A for five wafers cut from different axial position (denoted by g, which is the fraction of the melt that has crystallized) (b) The radial distribution of indium in germanium crystal B for five wafers cut from different axial position g.

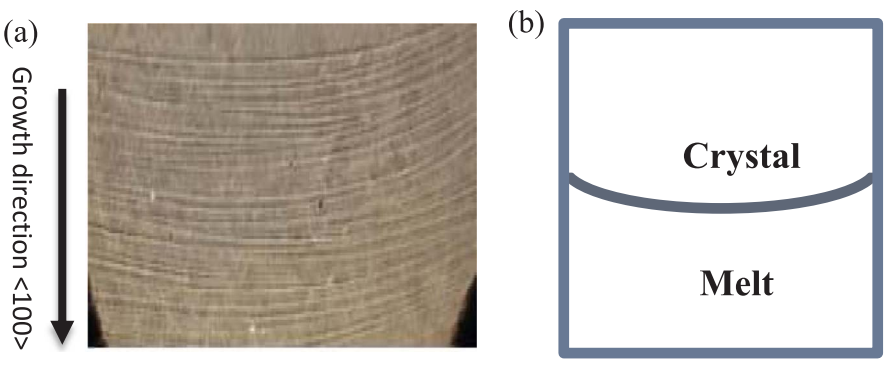

Fig. 4. (a) Microscopic striation analysis in a slice cut parallel to the growth axis taken from the neck part of Ge crystal. The area shown is 300 × 400 μm^2. (b) The interface morphology between crystal and melt.

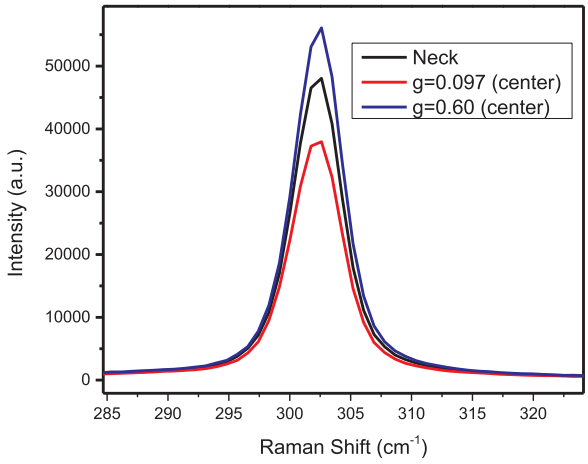

Fig. 5. The Raman spectra from neck, and centers of g = 0.097 and g = 0.60 wafers of crystal A.

Table 2
The Raman shifts residual stress and dislocation densities of three positions in crystal A.

Sample position	Raman peak shift (cm^{-1})	Stress (Kbar)	Dislocation density (cm^2)
neck	1.5	0.60	3300
g = 0.097	1.55	0.62	5800
g = 0.060	1.64	0.65	7500

K_{eq} is the equilibrium constant for a reaction. Based on the Gibbs free energy data [35], the Gibbs free energy data for indium concentration with 3 × 10^{12} and 1 × 10^{19} cm^{-3}, respectively, at 1210 K was calculated and listed in Table 3. The values of Gibbs free energy for four possible reactions are positive and indicate indium cannot react with SiO_2.

A wafer was located between the bottom of interface g_1 and the edge of interface g_2, as shown in Fig. 8. The indium concentration ratio of center and edge samples has then the form

$$\frac{N(g_1)}{N(g_2)} = \left(\frac{1-g_1}{1-g_2}\right)^{k-1} \tag{13}$$

The height of interface g_2 between center and edge is h.

$$h = \frac{4m}{\rho\pi D^2} - t \tag{14}$$

where m is the mass between interface g_1 and g_2; ρ is the density of germanium (5.323 g/cm^3), D is the diameter of wafer; t is the thickness of wafer. We ignore the non-uniformity distribution of indium in center sample and edge sample. Assuming $N(g_1) = N_{center}$ and $N(g_2) = N_{edge}$, then we calculated the heights of interface g_2 at different axial location according to Eqs. (13) and (14) and listed them in Table 1. The interface heights are dramatically decreased when $0.4 < g < 0.91$ for both crystals. The decrease of interface height indicates the axial thermal gradient is decreasing, which is caused by the decreasing mass of melt.

5. Conclusion

Two indium doped < 100 > germanium crystals were grown by CZ method from a quartz crucible under hydrogen atmosphere. The Hall mobility and concentration of indium were measured by Hall effect measurement at 77 K. The Hall mobility for two crystals shows good consistence with the theoretical calculation by B-H model. The concentrations of indium in grown crystals are in the range of 3 × 10^{12}~1 × 10^{19} cm^{-3}. The effective segregation coefficient of indium was calculated to be 0.0009, which indicates there is no evident indium-oxygen complex that has effect on the segregation of indium. The radial distribution of indium is caused by the small segregation coefficient of indium and the interface shape between crystal and melt in germanium crystals. The relationship between radial distribution of indium and interface shape was analyzed. The interface heights are dramatically decreased when $0.4 < g < 0.91$ for both crystals. The decrease of interface height is caused by the decrease of axial thermal gradient. The

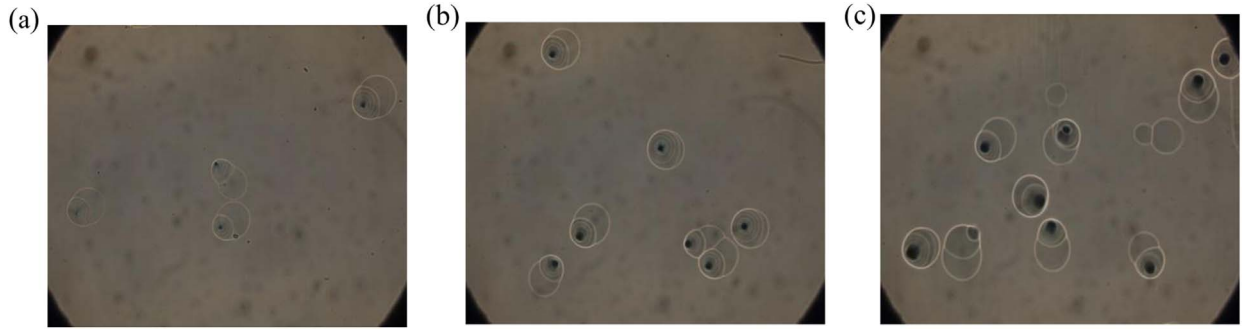

Fig. 6. The dislocations in the neck, g = 0.097, and g = 0.60 of the crystal A. For these images, the area shown is 300 × 400 μm^2. The dislocation densities are 3300, 5800, and 7500 cm^{-2}, respectively.

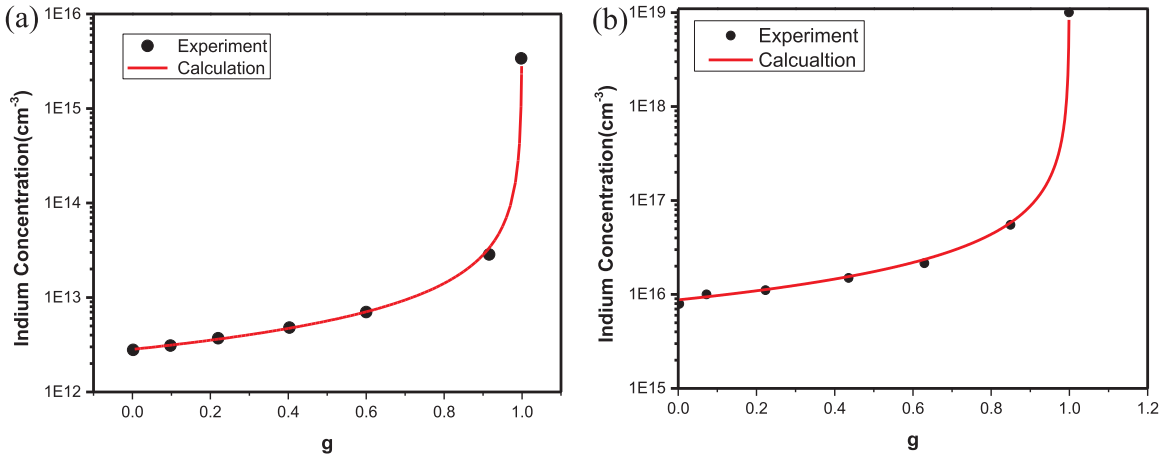

Fig. 7. (a) The measured axial distribution of indium in Ge crystal A (b) The measured axial distribution of indium in Ge crystal B.

Table 3
The possible chemical reactions between indium and silica during crystal growth and their corresponding standard Gibbs free energy $\Delta G^{\circ}_{(1210\ K)}$ and Gibbs free energy for indium concentration with 3×10^{12} and 1×10^{19} cm^{-3}, respectively, at 1210 K.

Reaction	$\Delta G^{\circ}_{(1210\ K)}$ (KJ/mol)	$\Delta G_{(1210\ K)}$ (KJ/mol) ($N = 3 \times 10^{12}\ cm^{-3}$)	$\Delta G_{(1210\ K)}$ (KJ/mol) ($N = 1 \times 10^{19}\ cm^{-3}$)
$2In + 3SiO_2 = 3SiO + In_2O_3$	930.7	465	767
$2In + SiO_2 = SiO + In_2O$	353.3	824	522
$4In + 3SiO_2 = 3Si + 2In_2O_3$	1007.1	749	900
$4In + SiO_2 = Si + 2In_2O$	421.6	629	478

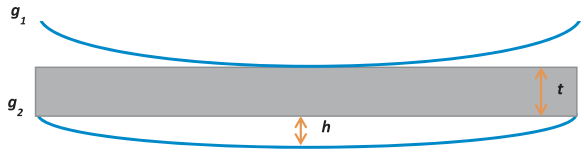

Fig. 8. The cross-section view of a wafer (grey), which is located between two interface shapes g_1 and g_2 (blue). (For interpretation of the references to color in this figure legend, the reader is referred to the web version of this article.)

normal segregation of indium in germanium makes it be a dopant candidate for growing p type high purity germanium crystals.

Acknowledgement

This work is supported by NSF OIA-1738632, DOE (Department of Energy) Grant DE-FG02-10ER46709 and the State of South Dakota.

References

[1] A. Chroneos, H. Bracht, R.W. Grimes, B.P. Uberuaga, Appl. Phys. Lett. 92 (2008) 172103.
[2] R. Kube, H. Bracht, A. Chroneos, M. Posselt, B. Schmidt, J. Appl. Phys. 106 (2009) 063534.
[3] A. Chroneos, R. Kube, H. Bracht, R.W. Grimes, U. Schwingenschlögl, Chem. Phys. Lett. 490 (2010) 38–40.
[4] R. Feng, F. Kremer, D.J. Sprouster, S. Mirzaei, S. Decoster, C.J. Glover, S.A. Medling, J.L. Hansen, A. Nylandsted-Larsen, S.P. Russo, M.C. Ridgway, J. Appl. Phys. 119 (2016) 025709.
[5] R.N. Hall, J. Phys. Chem. 57 (1953) 836–839.
[6] F.A. Trumbore, Bell Syst. Tech. J. 39 (1960) 205–233.
[7] G. Wang, M. Amman, H. Mei, D. Mei, K. Irmscher, Y. Guan, G. Yang, Mater. Sci. Semicond. Process. 39 (2015) 54–60.
[8] G. Wang, Y. Guan, H. Mei, D. Mei, G. Yang, J. Govani, M. Khizar, J. Cryst. Growth 393 (2014) 54–58.
[9] G. Yang, J. Govani, H. Mei, Y. Guan, G. Wang, M. Huang, D. Mei, Cryst. Res. Technol. 49 (2014) 269–275.
[10] J.S. Blakemore, Philos. Mag. 4 (1959) 560–576.
[11] H. Fritzsche, Phys. Rev. 99 (1955) 406–419.
[12] V.A. Moskovskih, P.V. Kasimkin, V.N. Shlegel, Y.V. Vasiliev, V.A. Gridchin, O.I. Podkopaev, J. Cryst. Growth 401 (2014) 767–771.
[13] M. Roth, M. Azoulay, G. Gafni, M. Mizrachi, J. Cryst. Growth 99 (1990) 670–675.
[14] G.S. Hubbard, E.E. Haller, W.L. Hansen, IEEE Trans. Nucl. Sci. 25 (1978) 362–370.
[15] W.L. Hansen, Nucl. Instrum. Methods 94 (1971) 377–380.
[16] W.L. Hansen, E.E. Haller, IEEE Trans. Nucl. Sci. 21 (1974) 251–259.
[17] H.W.H.M. Jongbloets, J.H.M. Stoelinga, M.J.H. van de Steeg, P. Wyder, Phys. Rev. B 20 (1979) 3328–3332.
[18] W.L. Hansen, E.E. Haller, MRS Proc. 16 (1982) 1–16.
[19] G. Wang, Y. Sun, G. Yang, W. Xiang, Y. Guan, D. Mei, C. Keller, Y.D. Chan, J. Cryst. Growth 352 (2012) 27–30.
[20] G. Wang, H. Mei, D. Mei, Y. Guan, G. Yang, J. Phys. Conf. Ser. 606 (2015) 012012.
[21] E.M. Conwell, Proc. IRE 40 (1952) 1327–1337.
[22] P.P. Debye, E.M. Conwell, Phys. Rev. 93 (1954) 693–706.
[23] F.J. Morin, Phys. Rev. 93 (1954) 62–63.
[24] D.M. Brown, R. Bray, Phys. Rev. 127 (1962) 1593–1602.
[25] IEEE Std 1160-1993 (1993) 36.
[26] D. Chattopadhyay, H.J. Queisser, Rev. Mod. Phys. 53 (1981) 745–768.
[27] H. Mei, D.M. Mei, G.J. Wang, G. Yang, J. Instrum. 11 (2016) P12021.
[28] E.M. Conwell, Phys. Rev. 103 (1956) 51–61.
[29] R.G. Sparks, M.A. Paesler, Precis. Eng. 10 (1988) 191–198.
[30] R.G. Sparks, W.S. Enloe, M.A. Paesler, Precis. Eng. 13 (1991) 189–195.
[31] J.H. Parker, D.W. Feldman, M. Ashkin, Phys. Rev. 155 (1967) 712–714.
[32] H. Fritzsche, M. Cuevas, Phys. Rev. 119 (1960) 1238–1245.
[33] W.G. Pfann, Trans. AIME 194 (1952) 747–753.
[34] K. Weiser, J. Phys. Chem. Solids 7 (1958) 118–126.
[35] I. Barin, Thermochemical Data of Pure Substances, Second ed, VCH, Weinheim, 1993, pp. 1480–1505.